Flexible resins lattices produced by stereolithography for biomedical applications

Stefano Belcuore[1,a], Stefano Pandini[1,b] Elisabetta Ceretti[1,c] and Paola Ginestra[1,d*]

[1]Department of Mechanical and Industrial Engineering, University of Brescia, Via Branze 38, 25123, Brescia (BS), Italy

[a]stefano.belcuore@studenti@unibs.it, [b]stefano.pandini@unibs.it, [c]elisabetta.ceretti@unibs.it, [d]paola.ginestra@unibs.it

Keywords: Lattice Structures, Flexible Resin, Stereolithography

Abstract. Stereolithography offers a promising solution to produce bespoke structures as surgical guides, models, and implants. The high aspect ratio of the obtained samples combined with different and tailorable mechanical properties make this technique very suitable for 3D-printed medical solutions. However, the epoxy resins used for this technology are toxic and need to be cured and washed very carefully to be used in contact with biological tissues. Most of the time these materials are used for orthoses and external structures instead of implants or tissue engineering scaffolds. Nowadays, lattice structures are achieving specific attention due to the possibility of tailoring the mechanical properties with lightweight geometries that can be 3D printed with several materials. The drawback point is that all the biomedical resins are rigid and show a fragile, although with relatively high maximum stress values, behavior. Moreover, it is even more difficult to fabricate both a flexible and a transparent part, especially by lithography polymerization, and transparent materials are usually required for certain biomedical applications. In this paper, we wanted to obtain a lattice structure that can be suitable for silicon liners as part of knee external prostheses with a flexible biocompatible, and transparent resin.

Introduction

Assuming a cubic structure when is subjected to compression, there is ideally a strictly linear correlation between the decrease in height with the expansion of width, this behavior is very common in most structures and is identified by a numerical value called Poisson's ratio, which for the case just mentioned is strictly positive. There are materials in nature, such as cork, which when subjected to compression show only a decrease in height therefore there is no expansion in width, this behavior is identified by the null value of the Poisson ratio. Other structures, on the other hand, have a negative value of the Poisson ratio, this means that at the time of their compression, the height decreases together with the width, while during traction both the value of the width and the height increases, this behavior defines a family of materials that are called auxetics. The main feature is the realization of mechanical metamaterials with textured and programmable functionalities, obtained through an anisotropic cubic block structure or "voxels" [1,2]. Additive manufacturing more commonly known as 3D printing is a process technology that allows you to create geometries starting from a three-dimensional CAD model, unlike more conventional subtractive technologies, additive manufacturing consists of overlapping various layers of material until the total creation of the solid [3,4,5]. The printing technologies often used for printing complex and high aspect ratio structures, are MSLA ((Masked Stereolithography Apparatus), SLA (Stereolithography), and DLP (Direct Light Processing) whose process is completely different from that of material extrusion, since the starting material is in a liquid state, the structure of the machine has only one degree of freedom or the z-axis on which the printing plate is positioned, and the material solidifies through a cross-linking process started by a light source positioned on the bottom of the machine [5]. The first technology analyzed is the MSLA type where the light

source generates a light with a wide beam that is masked by an LCD screen, placed above it, to filter and project only a cross-section of the CAD in contact with the resin. The second technology is SLA, the technologies are very different from each other, in this case, the SLA technology is composed of at least one laser that projects a very precise light beam that linearly solidifies the entire surface of the CAD cross-section directly in contact with the resin. The third technology analyzed is DPL, conceptually it is a compromise between the first two as the light source is neither a lamp masked with a screen nor a direct laser, but rather a projector that illuminates the resin directly with the CAD cross-section. This solution is closer to the concept of MSLA, but the constraint of the masker screen has been eliminated. All three types of 3D printers have their aspects, MSLA and DLP technologies are much faster than SLA as illuminating a small portion of resin or a large one, through direct projector or masking, does not involve any temporal variation of the process, on the other hand, the precision that a laser beam can guarantee is not reachable for the other techniques. In SLA and all technologies that use liquid resins, after the geometry has been created, the first thing to do is to clean the residual resin on its surface through a bath in isopropyl alcohol, for a time defined by the material used for printing, then a drying and curing process is carried out. In order, drying consists of drying the specimen through a heating ramp and maintaining it at a temperature, that also varies with the type of resin used, then moving on to the final step, i.e. curing, through ultraviolet light beams, that illuminates the entirety of the geometry, thus definitively polymerizing the whole sample.

In this paper, a 3D lattice six-hole buckling structure was designed in Inventor Professional (2023, ©1982-2024 Autodesk) varying the geometrical parameters to evaluate the manufacturing process. The Prusa SL1 (© Prusa Research a.s.) and Formlabs 3BL (© Formlabs 2024). We managed to parametrize the CAD model by imposing only three dimensions on the structure. The viscosity of the resin must be considered in the design of the structure along with the correct exposure times. The stresses introduced during the production process can deform and damage the structure, as this resin allows considerable deformations. The structure must include design structures that involve and take into account the required lattice geometry about the technological limitations of the process. Moreover, in this case, a flexible resin has been used for the production of the samples considering the limitations imposed by the process when flexible polymers are used [6]. Flexible and transparent resins, if biocompatible, are considered difficult and yet-to-be-optimized materials to be processed by stereolithography [7], thus assuring a certain degree of precision and dimensional accuracy, for bespoke biomedical designs.

Materials and Methods

The metamaterial studied and realized in this research is a bucklicrystal, in particular, it is a 3D auxetic lattice, designed by assembling the 6-hole units in the cubic crystal systems of the body center cubic (BCC)(1), with brevity the structure is defined as BCC-6H or Six-hole Bucklicrystal (2). This structure is characterized by the great variation in volume following compression thanks to the controlled collapse of its cells, this behavior makes lattice very similar to the use of elastic materials, thanks to their ability to undergo large deformations.

The creation of the three-dimensional CAD model is one of the key phases during the analysis of this type of structure, we will report several iterations of this geometry progressively making changes aimed at improving the 3D printing process. The software used to draw each metamaterial made and reported in this research is Inventor Professional (version 2023, ©1982-2025 Autodesk).

The first cell “1”, was a cube of 7 mm side in which a sphere of 6,348 mm in diameter was concentrically inserted as a pore, the external cube was inscribed in a circle that through revolution smoothed the vertices and a 45° taper angle was used on all the side faces.

Cell “2” is the first evolution, in fact, it was obtained through a uniform scale factor of 120% to strengthen the structure as the thin vertical walls did not withstand the forces that occurred during the production process.

Cell “3” was a further attempt to strengthen the structure, it is the direct evolution of cell 2 to which the side holes were reduced. This change made the printing process more repeatable and gave the final structure greater stiffness.

The cells are the repeating basic unit within the structure, different types of cells have been made and a unit cell with an internal pore diameter of 7.6 mm and side of 8.4 mm has been chosen as the base of further parameterization. To obtain a six-hole bucklicrystal structure, the cell listed above must be placed in a BCC (body center cubic) lattice, thus creating a three-dimensional structure in which a six-hole cell is positioned in each lattice node. Various structures have been created to obtain a repeatable result over time, below are the tabulated data of all the various iterations (Fig. 1, Fig. 2, and Fig. 3).

Lattice 1. The first iteration places cell 1 in a BCC lattice to which two compression planes are added, as a design item for future mechanical characterizations, 2mm thick. The structure made with the following parameters showed adhesion problems between the plates and the lattice itself, the interface area is not sufficient to withstand the forces present during the production process (Fig.1).

Lattice 2. The second iteration has the task of solving the critical issues encountered with the first structure. The scale factor applied on cell 2 has been maintained on the BCC lattice, thus obtaining the same previous structure but with a global scale factor of 120%. The changes made have not achieved the desired goal, the structure resists better to the stresses of the process but not uniformly throughout the lattice (Fig.1).

Lattice 3. The third interaction focuses on the most critical region of the structure, i.e. the interface area between the compression plates and the grating, thus adding 2 fittings, one on the external side and one on the internal side of the cell, thus increasing the contact area. The modification made was successful but showed other critical areas, in particular, the four columns that make up the cell are too thin and not very resistant to tensile force (Fig. 1).

Lattice 4. The fourth iteration definitively solves the problem of poor adhesion, to do this all the side pores of the repeating cell in contact with the compression plates were removed (Fig.2).

Lattice 5. The fifth iteration makes a substantial change compared to the previous lattice, as the repeating base unit has changed, the new cell has a lower porosity which guarantees it greater robustness; in fact, one of the most critical points that characterized all the previous grids were the four side columns of the cell. This change to the structure made the process less variable and more repeatable over time (Fig.2).

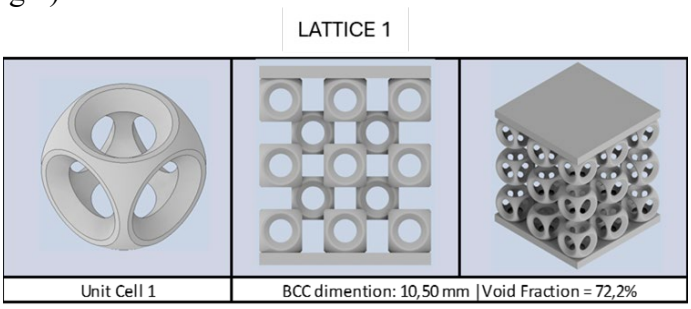

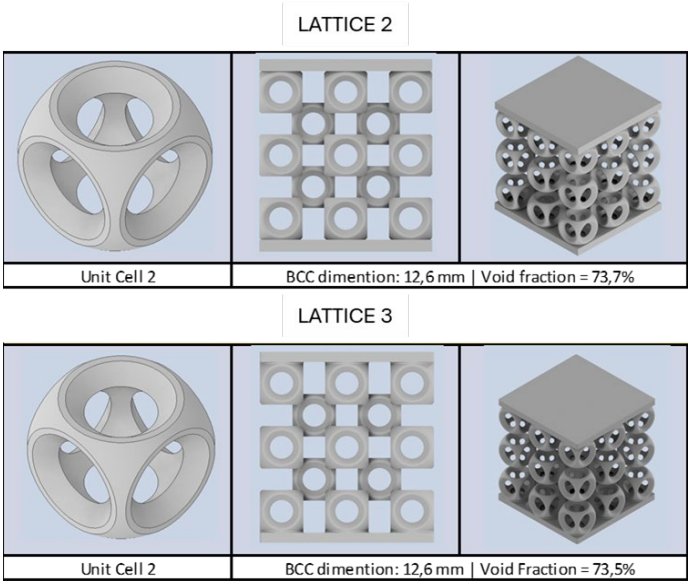

Figure 1 – Representation of Lattice 1, 2, and 3 in relation to each cell design chosen.

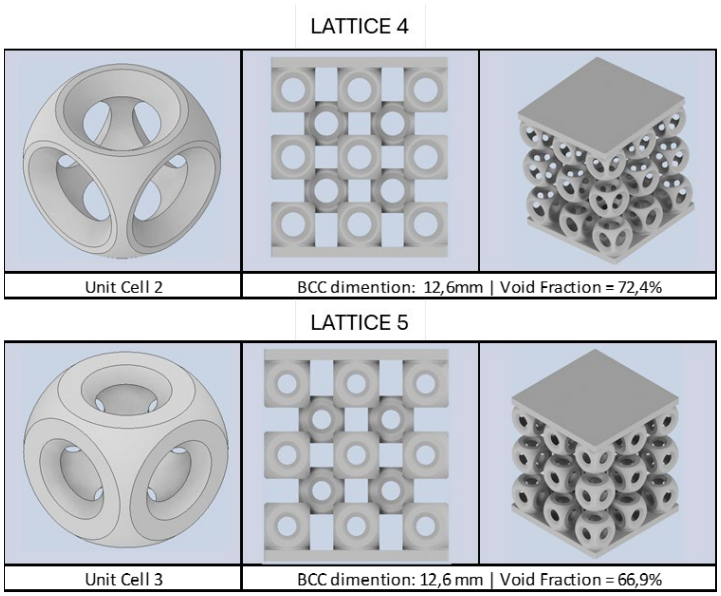

Figure 2 – Representation of Lattices 4 and 5 in relation to each cell design chosen.

Final structure. The final iteration brings quarter cells to support the outer cells, the basic structure to which these changes have been made is the same as the last iteration (Fig. 3).

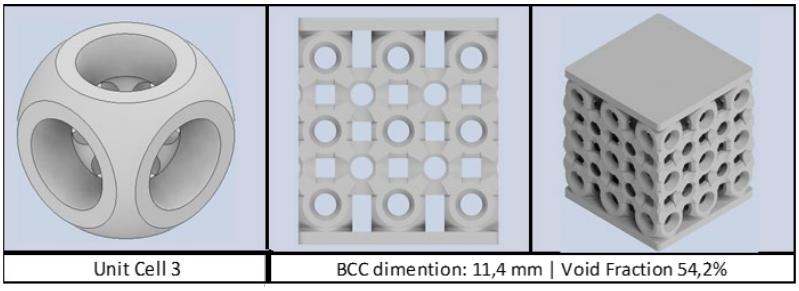

Figure 3 – Representation of the Final Lattice Structure in relation to the final cell design.

For the production of the lattice structures from number 1 to the final structure, a Prusa SL1 (MSLA), equipped with an LCD screen that masks the light beam coming from the source placed inside the body of the printer was used. The Prusa set parameters were 0.035 layer thickness and

20 seconds/layer of exposure time. For the production and comparison of the sole final structure, both the Prusa SL1 and the Formlabs 3BL (SLA), equipped with two laser sources that photo-cross-link the polymer, are used. The Formlabs set parameters were 0.1 layer thickness and 20 seconds/layer of exposure time (calculated as a medium time, considering the fixed printing parameters depending on the material cartridge). The Formlabs BioMed Elastic 50A Resin has been used with both printers. The Elastic 50A is a soft and elastic photo crosslinking resin designed for medical use, suitable for applications that require comfort, biocompatibility, and transparency. This material complies with ISO 10993 and is USP Class VI certified. It can be used in applications intended for long-term contact with the skin (> 30 days) and short-term contact with mucous membranes (< 24 hours). The post-trial treatment was divided into three temporally distinct phases, each lasting 10 minutes. The first phase is Washing, the piece is immersed in a container containing isopropyl alcohol and magnetically stirred, then follows the Drying phase in which the piece is dried at a constant temperature and finally Curing completes the partial cross-linking of the piece.

After the creation of the lattices, it was decided to proceed with the dimensional analysis of the various samples using the Quick Scope Mitutoyo optical microscope, which made it possible to verify and highlight the geometric deviations from the CAD and emphasize the process defects in the most critical areas of the geometry.

As previously explained, two different technologies were used for the realization of the specimens, subsequently the dimensional accuracy will be compared as the two technologies vary.

To have a valid statistical correlation, it was decided to choose critical quota values that can be easily measured on the cell, to minimize human error during measurement. The parameters to be measured are the left and right side thicknesses, the total width, and the values of the diameter of the cell in X-axis and Y-axis directions, after which the average for each cell for each of the three measurements and the standard deviation of the measurements from the latter are calculated.

Results

The following images show the structures obtained by the Prusa SL1 printer, specifically lattices 2,3,4 and 5, while lattice 1 did not result in any product to be shown (Fig. 4). The lattices 2 and 3 were not used for the geometry measurements due to the poor printing quality observed on the specimens (Fig. 6).

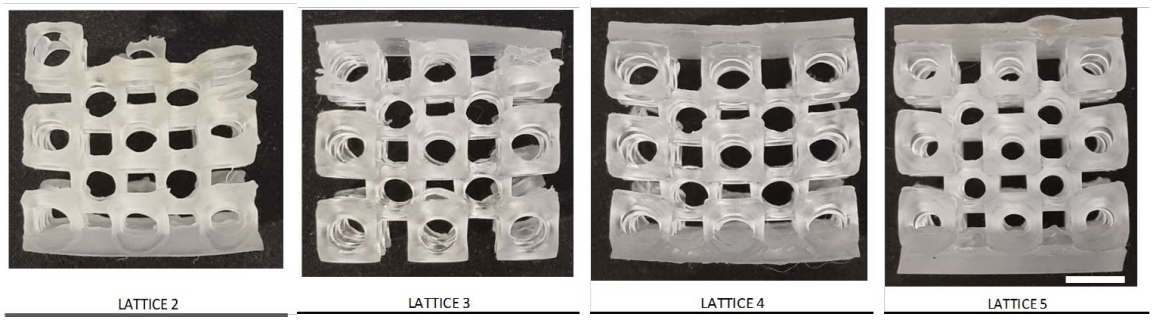

Figure 4 – Samples produced with Prusa SL1 with different lattice designs. The scale bar is 5 mm.

The final structure is shown in the comparison between the products obtained with the Prusa SL1 and the Formlabs 3BL printers (Fig. 5).

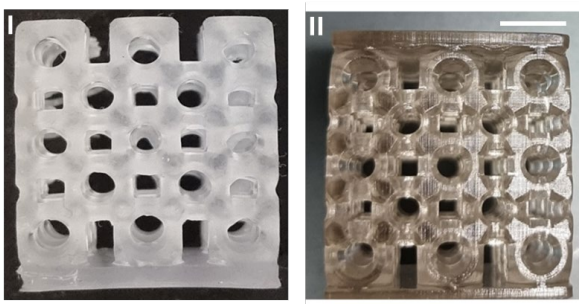

Figure 5 – Final lattice structure produced with Prusa SL1 (I) and Formlabs 3BL (II). The scale bar is 5 mm.

The measurements results are reported in the following graphs that show the threshold target, i.e. the corresponding CAD, as a horizontal red bar, for reference.

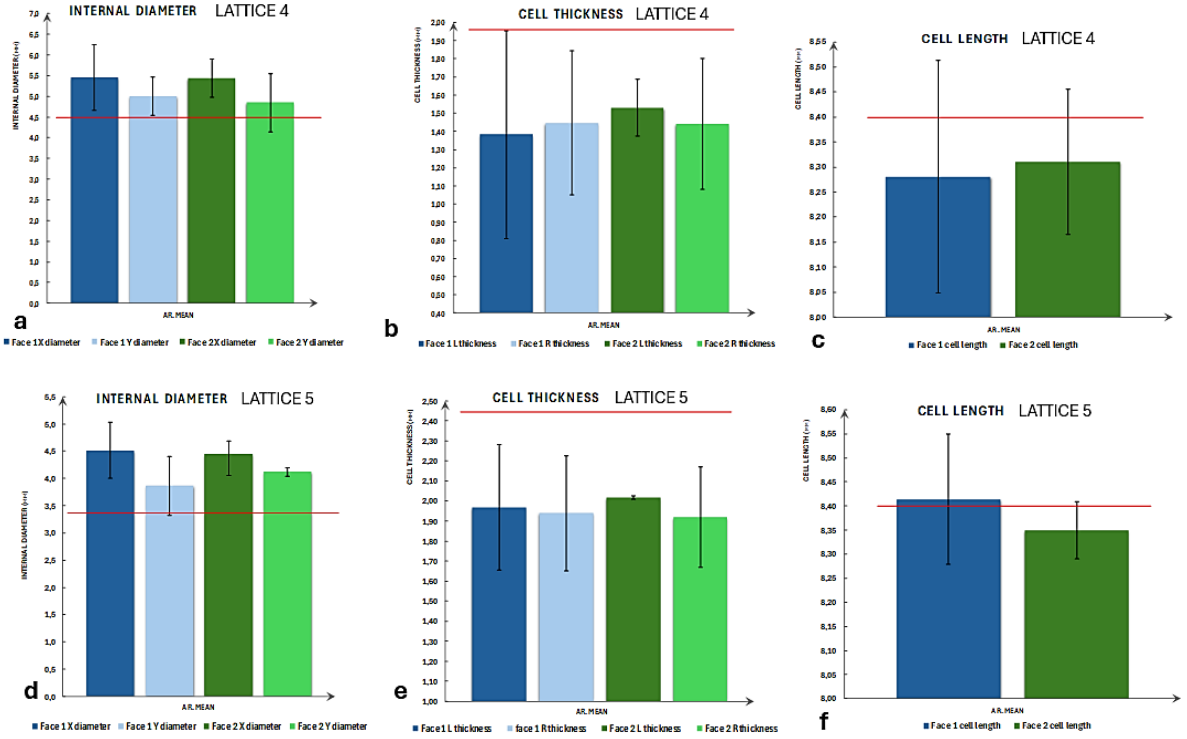

Figure 6 – Graphs reporting the geometrical features measured on Lattice 4 and 5 as a reference of the Prusa SL1 stability for the production of these structures. The horizontal red bar is referred to the CAD target value. Internal Cell Diameter measured on Lattice 4 and 5 (a,d); Cell Thickness measured on Lattice 4 and 5 (b,e) and Cell total length measured on Lattice 4 and 5 (c,f). a) red bar at 4.47 mm; b) red bar at 1.96 mm; c) red bar at 8.40 mm; d) red bar at 3.44 mm; e) red bar at 2.48 mm and f) red bar at 8.40 mm.

From the graph in Fig. 6 representing the cells geometrical features measured each time on the X and Y directions of two faces of each structure (i.e. to enhance the statistical significance of the measurements). Fig. 4a and 4d report internal diameter of the cells it can be seen that all the average values are above the CAD value and that the diameters measured on the X-axis are always greater than those measured on the Y-axis, implying that the pore is not only elliptical but also larger than the expected pore. This behavior is due to the strength and amount of material from which the cell is made since the "LATTICE 4" lattice uses a type "2". The standard deviation also increases as the thinner walls of cell "2" give less stability to the creation of the subsequent layers of material.

Fig. 4 b and e reporting the lateral thicknesses (i.e. width of the cell side) of the cell, shows how the latter are significantly below the design value, thus confirming the cause of the increase in the standard deviation following a lack of robustness of the structure.

Finally, the total width of the cells (Fig. 4 c and f) reveals that it is also below the design value, although by a much lower value than the deviations shown in the previous graphs. It can be concluded that a certain balance has been established between the increase in the diameter of the internal pore and the thicknesses of the lateral opinions, thus keeping the value of the total width of the cell close to that of the design. Fig. 6 reports the measurements made on the lattice "LATTICE 5" where the cell used is type "3" and has a porosity lower than the type "2" cell. Despite the lower porosity of "LATTICE 4", the results are comparable and share the same conclusions, but a slight decrease in the standard deviation can be noted, especially in the graph representing the thicknesses of the side walls.

The following image (Fig.7) always shows the results of the measurements made on the lattice "FINAL LATTICE" made with the Prusa SL1. This lattice has been specially replicated with the two different types to compare the differences in the finished product with the same geometry. This time, the measurements were taken on two subsequent faces of the structure to take the printing direction into account.

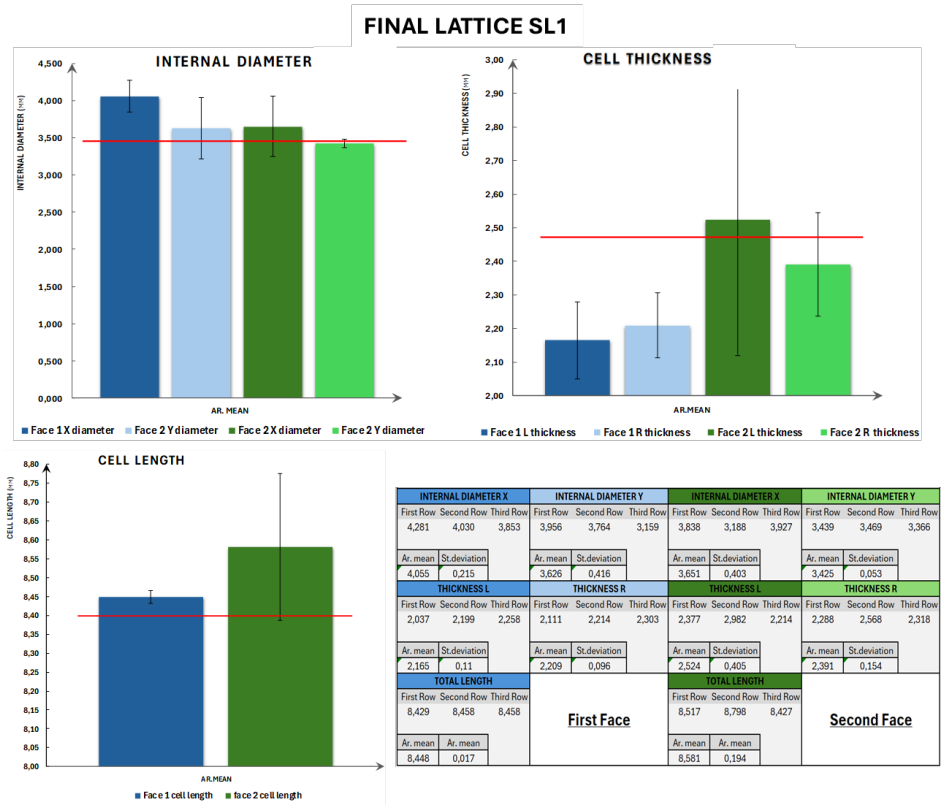

Figure 7 – Graphs reporting the geometrical features measured on the Final Lattice Structure printed with the Prusa SL1. The horizontal red bar is referred to the CAD target value. Internal Diameter Red Bar at 3.45 mm; Cell Thickness Red Bar at 2.47 mm and Cell Length Red Bar at 8.40 mm. The Table shows the mean and standard deviation values for all the analyzed samples.

Analyzing in order the graphs on the internal diameter followed by the wall thickness and finally the total width of the cells, it can be seen that the diameter measured on the Y-axis is always smaller than that measured on the X-axis, which implies that all the pores are elliptical with the largest diameter placed on the X-axis. It is also clear that the Y diameters are much closer to the geometric value of the CAD, as opposed to the previous case, showing greater accuracy than the

X diameters. The difference between the standard deviation of the measurements is very marked. Concerning the thickness of the cell walls, no particular trend is reported except that all the average values are very far from each other and below the threshold value of the CAD, except in one case, however, it can be deduced that the standard deviation values are higher than those reported in the graph of diameters.

Finally, the graph representing the total width of the cells shows how the average of the cells measured on both faces is higher than the threshold value and with a marked deviation on one of the two faces. The following image always shows the results of the measurements made on the lattice "FINAL LATTICE" made with the Formlabs 3BL (Fig. 8).

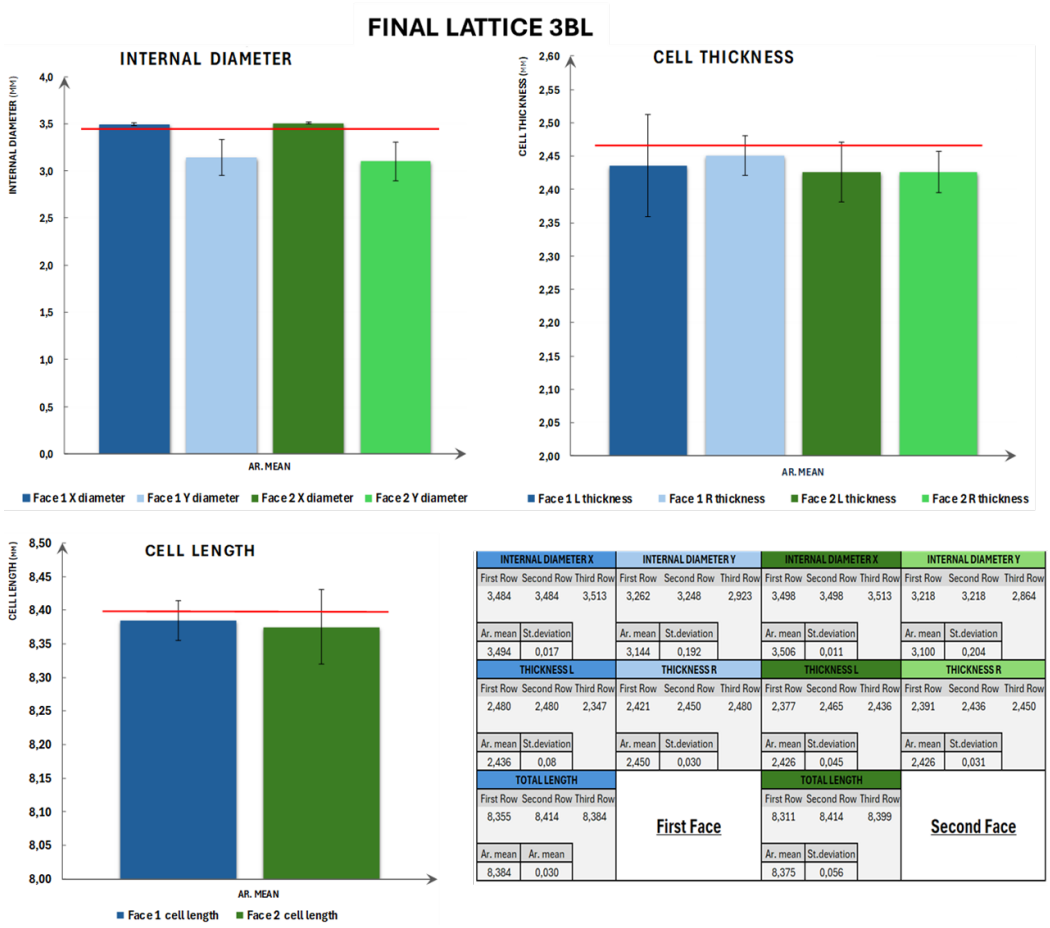

INTERNAL DIAMETER X			INTERNAL DIAMETER Y			INTERNAL DIAMETER X			INTERNAL DIAMETER Y		
First Row	Second Row	Third Row	First Row	Second Row	Third Row	First Row	Second Row	Third Row	First Row	Second Row	Third Row
3,484	3,484	3,513	3,262	3,248	2,923	3,498	3,498	3,513	3,218	3,218	2,864
Ar. mean	St.deviation		Ar. mean	St.deviation		Ar. mean	St.deviation		Ar. mean	St.deviation	
3,494	0,017		3,144	0,192		3,506	0,011		3,100	0,204	
THICKNESS L			THICKNESS R			THICKNESS L			THICKNESS R		
First Row	Second Row	Third Row	First Row	Second Row	Third Row	First Row	Second Row	Third Row	First Row	Second Row	Third Row
2,480	2,480	2,347	2,421	2,450	2,480	2,377	2,465	2,436	2,391	2,436	2,450
Ar. mean	St.deviation		Ar. mean	St.deviation		Ar. mean	St.deviation		Ar. mean	St.deviation	
2,436	0,08		2,450	0,030		2,426	0,045		2,426	0,031	
TOTAL LENGTH						TOTAL LENGTH					
First Row	Second Row	Third Row				First Row	Second Row	Third Row			
8,355	8,414	8,384	First Face			8,311	8,414	8,399	Second Face		
Ar. mean	Ar. mean					Ar. mean	St.deviation				
8,384	0,030					8,375	0,056				

Figure 8 – Graphs reporting the geometrical features measured on the Final Lattice Structure printed with the Formlabs 3BL. The horizontal red bar is referred to the CAD target value. Internal Diameter Red Bar at 3.45 mm; Cell Thickness Red Bar at 2.47 mm and Cell Length Red Bar at 8.40 mm. The Table shows the mean and standard deviation values for all the analyzed samples.

Analyzing in order the graph on the internal diameter followed by that of the wall thickness and finally the total width of the cell, it can be seen that the diameter measured on the Y-axis is always smaller than that measured on the X-axis, which implies that all pores are elliptical with the largest diameter placed on the X-axis. It is also clear that the X diameters are much closer to the geometric value of the CAD showing greater precision than the Y diameters, finally it can be seen how the trends of the values measured on one face are also reflected on the second.

As far as the graph showing the values of the thickness of the cell walls is concerned, no particular trend is reported except that all the average values are similar to each other and below the threshold value of the CAD, with very low standard deviation values.

Finally, the graph representing the total width of the cells shows that the average of the cells measured on both faces is less than the threshold value but with minimal deviation.

Conclusions

The study focused on the design, optimization, and production of 3D lattice structures using various stereolithography (SLA, MSLA) technologies, aimed at biomedical applications. Through iterative design changes, such as strengthening the geometry and improving the adhesion during the printing process, the structural integrity and printability of the six-hole Bucklicrystal (auxetic lattice) were significantly enhanced. The material used, Elastic 50A resin, proved to be crucial in ensuring the stability of the printed lattices, with exposure time and layer thickness playing a key role in the print quality.

Dimensional accuracy varied between the two printing technologies tested, with the Formlabs 3BL printer providing better results in terms of precision, especially with the X-axis diameters. The Prusa SL1 showed some discrepancies in wall thickness, internal diameter, and total width. However, both printers exhibited successful outcomes for the final lattice, though with some differences in geometric accuracy.

The Elastic 50A resin used in this study is suitable for long-term biomedical applications, with proven biocompatibility and transparency, making it appropriate for skin-contact medical devices. Post-processing steps like washing, drying, and curing were critical to achieving the desired final properties of the structures, ensuring their reliability for clinical use. The study underlines the importance of careful design, material choice, and process optimization to create functional 3D-printed lattice structures with potential biomedical applications.

Funding

This research was supported by the European Union - NextGenerationEU - Ministry of Research and University - PRIN (National Relevant Interest Projects) Code: 2022ATZTBS: Micro-manufacturing technologies for structured organ-on-chip (MITO). Mission 4,1. CUP D53D23003370006

References

[1] Chenxi Lu , Mengting Hsieh , Zhifeng Huang , Chi Zhang , Yaojun Lina, Qiang Shen , Fei Chen ,Lianmeng Zhang. W. (2022). Architectural Design and Additive Manufacturing of Mechanical Metamaterials: A Review. Engineering, 17, 44-63. https://doi.org/10.1016/j.eng.2021.12.023

[2] Shangqin Yuan, Fei Shena, Jiaming Bai, Chee Kai Chua, JunWei, Kun Zhou. 3D soft auxetic lattice structures fabricated by selective laser sintering: TPU powder evaluation and process optimization, W.(2017). Materials and Desing, 120,317-327. http://dx.doi.org/10.1016/j.matdes.2017.01.098

[3] Mussini Andrea, Carter Luke, Villapun Victor, Cao Emily, Cox Sophie, and Ginestra Paola. 3D printing for Growth Adaptive Medical Devices: an alternative approach for craniosynostosis (2024) Procedia CIRP, 125, 319-324. 10.1016/j.procir.2024.08.054

[4] Mussini Andrea, Carter Luke, Villapun Victor, Cao Emily, Cox Sophie, and Ginestra Paola. Experimental and computational analysis of 3D printed 2D lattices (2024) Materials Research Proceedings, 41, 390-397. 10.21741/9781644903131-44

[5] Riva Leonardo, Ginestra Paola Serena, Pandini Stefano and Pasini Chiara. Production and characterization of the Poisson's ratio of cellular structured metamaterials by additive manufacturing (2022) Procedia CIRP, 110, 380-384. 10.1016/j.procir.2022.06.067

[6] Tsai,Hung-Yin, Ceretti Elisabetta, Rizzi Davide, Ginestra Paola, Kao Tuan-Huan, Leu Ming. Laser-induced metallization on flexible polymer coating: Analysis and application (2021) Journal of Materials Processing Technology, 290, 116986. 10.1016/j.jmatprotec.2020.116986

[7] Riva Leonardo, Mazzoldi Elena Laura, Ginestra Paola Serena, Ceretti Elisabetta and Giliani Silvia Clara. Eye model for floaters' studies: production of 3D printed scaffolds (2022) Progress in Additive Manufacturing, 7, 1127-1140. 10.1007/s40964-022-00288-5